A Basic Approach Toward the Development of Nanocomposite Magnetic Scaffolds for Advanced Bone Tissue Engineering

R. De Santis,[1] A. Gloria,[1] T. Russo,[2] U. D'Amora,[1] S. Zeppetelli,[1] C. Dionigi,[3] A. Sytcheva,[4] T. Herrmannsdörfer,[4] V. Dediu,[3] L. Ambrosio[1]

[1]*Institute of Composite and Biomedical Materials, National Research Council, P. le Tecchio 80, 80125 Naples, Italy*
[2]*Department of Materials and Production Engineering, University of Naples "Federico II," P. le Tecchio 80, 80125 Naples, Italy*
[3]*Institute of Nanostructured Materials, National Research Council, Via P. Gobetti 101, Bologna 40129, Italy*
[4]*Helmhotz-Zentrum Dresden-Rossendorf (HZDR), Dresden High Magnetic Field Laboratory (HLD), P.O.-Box 51 01 19, D-01314, Dresden, Germany*

Received 28 April 2011; accepted 28 April 2011
DOI 10.1002/app.34771
Published online 10 August 2011 in Wiley Online Library (wileyonlinelibrary.com).

ABSTRACT: Magnetic scaffolds for bone tissue engineering based on a poly(ε-caprolactone) (PCL) matrix and iron oxide (Fe_3O_4) magnetic nanoparticles were designed and developed through a three-dimensional (3D) fiber-deposition technique. PCL/Fe_3O_4 scaffolds were characterized by a 90/10 w/w composition. Tensile and magnetic measurements were carried out, and nondestructive 3D imaging was performed through microcomputed tomography (Micro-CT). Furthermore, confocal analysis was undertaken to investigate human mesenchymal stem cell adhesion and spreading on the PCL/Fe_3O_4 nanocomposite fibers. The results suggest that nanoparticles mechanically reinforced the PCL matrix; the elastic modulus and the maximum stress increased about 10 and 30%, respectively. However, the maximum strain decreased about 50%; this suggested an enhanced brittleness. Magnetic results evidenced a superparamagnetic behavior for these nanocomposite scaffolds. Micro-CT suggested an almost uniform distribution of nanoparticles. Confocal analysis highlighted interesting results in terms of cell adhesion and spreading. All of these results show that a magnetic feature could be incorporated into a polymeric matrix that could be processed to manufacture scaffolds for advanced bone tissue engineering and, thus, provide new opportunity in terms of scaffold fixation and functionalization. © 2011 Wiley Periodicals, Inc. J Appl Polym Sci 122: 3599–3605, 2011

Key words: biocompatibility; polyesters; nanocomposites; nanoparticles

INTRODUCTION

Tissue engineering has been defined as a multidisciplinary field that integrates principles of engineering and life sciences to develop biological substitutes that restore, maintain, or improve tissue function.[1]

To achieve tissue regeneration, cell-based therapies, tissue-inducing factors, and biocompatible scaffolds have been investigated singularly and in combination.[2–15]

The most promising approach involves the cell seeding of three-dimensional (3D) porous and biodegradable scaffolds.

In the design of scaffolds for tissue engineering applications, the main ambition is to reproduce the function of the natural extracellular matrix to provide a temporary template for the growth of target tissues.[16]

It is well known that a scaffold has to satisfy several requirements[16–18] and show a set of chemical, biochemical, and biophysical material properties that are able to control and promote specific events at the cellular and tissue levels.[19] In particular, with regard to hard tissue engineering, such as bone, it appears clear that scaffolds should possess suitable mechanical properties and architecture to play their specific role.

Over the past years, great efforts have been made to develop technologies aimed at manufacturing scaffolds. In particular, the introduction of rapid prototyping technologies in the biomedical field has allowed for the division of scaffold fabrication techniques into two main groups, conventional and novel methods.[16,20,21]

However, with conventional manufacturing techniques, the precise control of the internal morphology and interconnectivity (i.e., pore size, pore geometry, spatial distribution of pores, internal channels) is strongly limited.[20–23]

Conversely, rapid prototyping can be considered as the main strategy able to produce customized scaffolds with a reproducible internal architecture.

Correspondence to: R. De Santis (rosantis@unina.it).

Rapid prototyping techniques allow one to obtain a higher degree of architectural control and, thus, enhances the transport of oxygen and nutrients throughout the scaffold.[16,20,24]

Data obtained from computed tomography or magnetic resonance imaging medical scans can be used to make a customized computer-aided design (CAD) model and, hence, a scaffold that should present the exact external shape required to correct the damaged tissue site.[20,22,25,26]

Among the rapid prototyping methods, the 3D fiber-deposition technique has emerged as a powerful tool for the manufacture of well-defined and custom-made scaffolds with 100% interconnected pores, also because of its flexibility in processing a wide range of materials.[16]

Natural, synthetic, semisynthetic, and hybrid materials have been proposed and studied to make scaffolds.[20,22,27–35] However, unlike natural polymers, synthetic polymers show several advantages, including flexibility and processability into different sizes and shapes.[36]

Among synthetic polymers, poly(ε-caprolactone) (PCL), a biodegradable aliphatic polyester, has already been considered for a wide range of applications, such as tissue-engineered skin, drug-delivery systems, and scaffolds for supporting fibroblast and osteoblast growth.[37–41]

In a further study on dynamic coseeding onto 3D fiber-deposited PCL scaffolds, Kyriakidou et al.[42] underlined how osteoblasts increase the proliferation of endothelial cells and how endothelial cells amplify the growth of osteoblasts but decrease their differentiation.

Moreover, as reported in the literature, many polymeric and composite materials have been considered to make porous scaffolds, also with the more advanced manufacturing methods (i.e., rapid prototyping techniques).[43]

Recently, it has been reported that nanotechnology may enhance the performance of all of the materials used for regrowing bone. This approach has led to the design of materials with nanostructured surface features or constituent nanomaterials, such as fibers, grains, or particles, that show at least one dimension from 1 to 100 nm. Nanomaterials highlight properties that are superior to those of their conventional bulk (or microstructured) counterparts as a consequence of novel physical properties also related to nanoscale features.[43–46]

The novel aspect of nanotechnology results in the design of materials that may reproduce the natural nanostructure of tissues. In the field of bone regeneration, the significant role of nanotechnology in improving the efficiency of polymer-based materials has been evidenced by several investigations.[43,44,47] Nanocomposites can mimic the constituents of natural bone better than the individual components, and the effect of nanoscale features on scaffold function and properties becomes important.[44,47] Natural bone can be considered a hierarchical material with the lowest level belonging to the nanoscale range. For this reason, materials with nanometer-sized structures seem to be natural choices for making scaffolds with enhanced properties for bone tissue engineering.[44]

Thus, nanocomposites consisting of a natural or synthetic polymer reinforced with an inorganic phase (i.e., ceramic phase) are increasingly preferred for bone tissue regeneration because they more closely mimic the structure of natural bone. In comparison with conventional composites, nanocomposites better induce cell response because of their similarity with the natural structure. Moreover, the mechanical performances of nanocomposites may also be further improved in comparison with conventional composites.[48]

In this context, many works suggest that better osteoconductivity can be achieved with synthetic composite materials that are similar in size and morphology to both the inorganic particles and organic phase of bone,[44,49,50] and bone cell functions seem to be better enhanced through interaction with nanophase ceramics and nanostructured polymers collectively rather than individually.[44,50–54]

A conceptually innovative solution for the design of magnetic scaffolds for tissue engineering was recently proposed.[55] This strategy aims to design magnetic scaffolds through the dip coating technique that are able to attract and take up *in vivo* growth factors, stem cells, or other bioagents bound to magnetic particles.

Accordingly, the aim of this research was to highlight an approach in the design and development of 3D fiber-deposited magnetic PCL/iron oxide (Fe_3O_4) scaffolds. We also investigated the effect of Fe_3O_4 nanoparticles on the biological, mechanical, and magnetic performances.

EXPERIMENTAL

Design and preparation of PCL/Fe_3O_4 nanocomposite scaffolds

PCL (weight-average molecular weight = 65,000, Aldrich, St. Louis, MO) pellets were dissolved in tetrahydrofuran with stirring at room temperature. Polyvinylpyrrolidone (PVP) coated Fe_3O_4 (99.5%, 25 nm, 0.2 wt % PVP, NanoAmor, Houston, TX) nanoparticles and then ethanol were added to the PCL/tetrahydrofuran solution during stirring. A PCL/Fe_3O_4 nanoparticles weight ratio (w/w) of 90/10 was used. An ultrasonic bath (Branson 1510 MT, Danbury, CT) was also used to optimize the Fe_3O_4

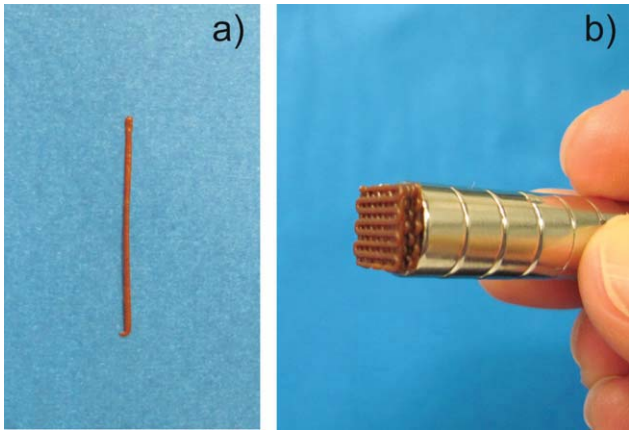

Figure 1 Optical images of an (a) nanocomposite fiber showing the capability of the 3D fiber-deposition process to realize straight fibers and (b) a magnetic scaffold attracted by a neodymium magnet. [Color figure can be viewed in the online issue, which is available at wileyonlinelibrary.com.]

nanoparticle dispersion in the polymer solution. Accordingly, a homogeneous paste was obtained, and then, the solvent was totally removed. Successively, PCL/Fe_3O_4 (90/10 w/w) pellets were made.

Nanocomposite fibers and 3D scaffolds with a 0°/90° pattern were preliminary manufactured by the processing of PCL/Fe_3O_4 (90/10 w/w) pellets through a 3D fiber-deposition technique.

In particular, we built nanocomposite scaffolds by extruding and alternatively depositing the fibers along the 0° direction and the 90° direction between two successive layers, thus obtaining a 0°/90° pattern. PCL/Fe_3O_4 (90/10 w/w) pellets were initially placed in a stainless steel syringe and then heated at a temperature of 130–140°C with a heated cartridge unit placed on the mobile arm of a bioplotter-dispensing machine (Envisiontec GmbH, Gladbeck, Germany). Successively, a nitrogen pressure of 8.5–8.9 bar was applied to the syringe through a cap. The nozzle used to extrude the PCL/Fe_3O_4 fibers was stainless steel characterized by an inner diameter of 400 μm. Scaffolds were characterized not only by the fiber diameter (depending on the needle diameter and/or the deposition speed) but also by the fiber spacing (strand distance, that is, center-to-center distance) and layer thickness, which influenced the overall pore size. A deposition speed of 30 mm/min was used.

Images of the PCL/Fe_3O_4 nanocomposite fibers and scaffolds are shown in Figure 1.

Tensile tests of the PCL/Fe_3O_4 nanocomposite fibers

Tensile tests of the PCL and PCL/Fe_3O_4 nanocomposite fibers [340–360 μm and 380 μm in diameter (D), respectively] were performed with an Instron 5566 dynamometer (Bucks, UK) equipped with a 10-N load cell. The length of the fiber between the grips was set to 20 mm. The fibers were tested at a constant crosshead speed of 50 mm/min, according to the standard practice ASTM D 3822. The engineering stress was obtained as the force measured by the loading cell divided by the total area of the fiber cross section: $A = \pi/4D^2$, whereas the strain was defined as the ratio between the vertical displacement (i.e., the elongation), assumed to be equal to the crosshead displacement, and the initial distance between the grips.

Statistical differences for the tensile modulus (E), maximum stress (σ_{max}), and maximum strain (ε_{max}) between the polymeric and nanocomposite groups were assessed with a one-way analysis of variance through the software package OriginPro 7 (OriginLab Corp., Northampton, UK).

Imaging analysis

Microcomputed tomography (Micro-CT) was performed at a resolution of 5.8 μm through a SkyScan 1072 system (Aartselaar, Belgium) with a rotational step of 0.9° over an angle of 180° to capture the image and, hence, shape and size of the polymer and nanocomposite fibers. Cross sections and 3D models of the nanocomposite fibers were then reconstructed with SkyScan's software package, Image J, and Materialise Mimics software (version 12.0, Materialise, Leuven, Belgium) for image analysis and visualization of the results from Micro-CT scanning.

Also, a Nikon Eclipse 80i microscope (Mellville, NY) equipped with a Nikon digital camera was used for optical imaging of the scaffolds.

Magnetization analysis

Magnetization measurements were performed in a Squid magnetometer (San Diego, CA) designed for the operation ranges $-7\ \mathrm{T} \le B \le +7\ \mathrm{T}$ and $1.8\ \mathrm{K} \le T \le 400\ \mathrm{K}$. First, direct-current magnetization and alternating-current susceptibility at low magnetic field (several millitesla (mT)) were measured as functions of temperature. The material revealed superparamagnetic behavior with a blocking temperature at about 250 K.

The field-dependent magnetization curve, which is of practical interest for biomedical applications, was taken at *in vivo* temperature conditions of $T = 310$ K. Assuming monodisperse particle size, we fitted the experimental curve with a Langevin function common for superparamagnetic behavior:

$$M = M_s\left(\coth(\mu_p H/k_B T) - k_B T/\mu_p H\right) \qquad (1)$$

where M_s is the saturation magnetization, μ_p stands for the magnetic moment of a particle, k_B is the Boltzmann constant, and T and H are the temperature and magnetic field.

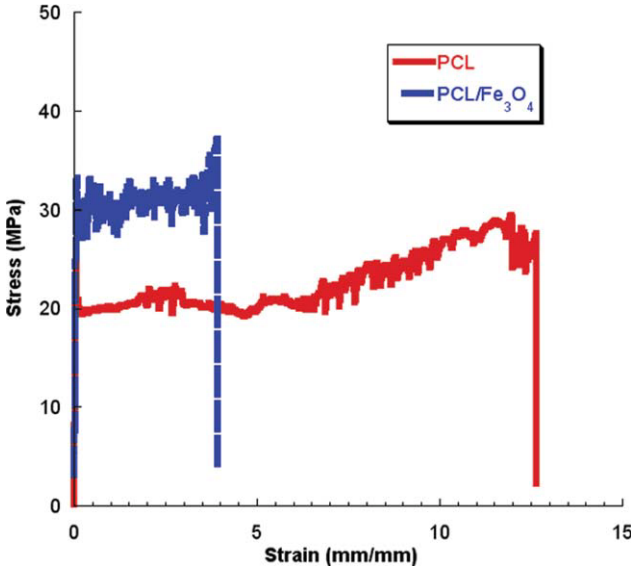

Figure 2 Typical stress–strain curves obtained from the tensile tests performed on PCL and PCL/Fe_3O_4 fibers. The increase of strength, but a decrease of strain to failure, can be detected for magnetic nanocomposite fibers. [Color figure can be viewed in the online issue, which is available at wileyonlinelibrary.com.]

Confocal laser scanning microscopy

Preliminary confocal laser scanning microscopy was carried out to study human mesenchymal stem cell adhesion and spreading on the PCL/Fe_3O_4 nanocomposite fibers at 72 h after seeding. To visualize the cells adhered to the nanocomposite fibers, the phalloidin-labeled actin filament fluorescence intensity was measured with several steps along the length of the fibers by means of a confocal laser scanning microscope (Zeiss LSM 510/Confocor 2, Oberkochen, Germany) equipped with argon and helium–neon laser sources at a wavelength of 543 nm and with a 20× objective. Images were acquired with a resolution of 512 × 512 pixels. The emitted fluorescence was detected with LP 560 and HFT 488/543 filters.

RESULTS AND DISCUSSION

Tensile tests of the PCL/Fe_3O_4 nanocomposite fibers

Figure 2 shows typical tensile stress–strain curves for the PCL and PCL/Fe_3O_4 fibers. In particular, the stress–strain curves obtained showed an initial linear region. Consecutively, a small decrease in the slope occurred up to a local σ_{max} value; this was followed by a decrease of the tensile stress. Then, it is worth noting that a plateaulike region and, finally, a new increase were observed until σ_{max} were reached.

E, σ_{max}, and ε_{max} are reported in Table I.

The results from the tensile tests evidenced a ductile behavior for both the PCL and PCL/Fe_3O_4 fibers. In particular, E obtained for the PCL fibers was consistent with the literature data;[42] however, the slightly greater value measured in this investigation may have been related to the higher speed of testing (50 mm/min).

Even though the inclusion of Fe_3O_4 nanoparticles strongly reduced ε_{max}, the results suggest that the modulus and σ_{max} were enhanced. The increases of stiffness and strength observed for PCL/Fe_3O_4 suggested that the use of 10 wt % magnetic nanoparticles was still an effective reinforcement, even if a maximum effect was expected at lower amounts of nanoparticles. However, the results from the statistical analysis highlighted a significant statistical difference between the polymeric and nanocomposite groups ($p < 0.01$) for both σ_{max} and ε_{max}, whereas a weaker difference ($p < 0.05$) was observed for E.

Furthermore, the values of E obtained for the fibers seemed to match those of trabecular bone;[56] this suggested the possibility of designing 3D fiber-deposited scaffolds for advanced bone tissue engineering by suitable selection of specific architectures and laydown patterns.

Imaging analysis

The first study step through Micro-CT involved the evaluation of the fiber diameter produced through a bioplotter, whereas the second one showed the distribution of Fe_3O_4 nanoparticle clusters. As for the diameter, the results evidence values of 340–360 and 380 μm for the PCL and PCL/Fe_3O_4 fibers, respectively. The images obtained through the Micro-CT system scan allowed for the 3D reconstruction of the nanocomposite fibers and, hence, the distribution of Fe_3O_4 nanoparticles (Fig. 3).

In particular, 3D reconstructions through Materialise Mimics highlighted an evident distribution of Fe_3O_4 nanoparticle clusters; thus, a uniform distribution of nanoparticles along each fiber composing the scaffold was expected. The clustering effect of high surface-to-volume ratio particles is widely documented; levels much lower than 10% already produce clusters. If clusters are effective for magnetic features of the scaffold, higher amount of clusters are known to drastically reduce the mechanical properties. The higher number of clusters, which can be detected from Figure 3, suggested that further increasing the amount of nanoparticles may lower mechanical properties. It is also interesting to

TABLE I
***E*, σ_{max}, and ε_{max} Values Reported as Mean Value ± Standard Deviation**

Fiber	E (MPa)	σ_{max} (MPa)	ε_{max} (mm/mm)
PCL	571.5 ± 45.6	29.3 ± 3.2	12.3 ± 2.0
PCL/Fe_3O_4	640.0 ± 60.4	38.1 ± 4.1	5.5 ± 1.4

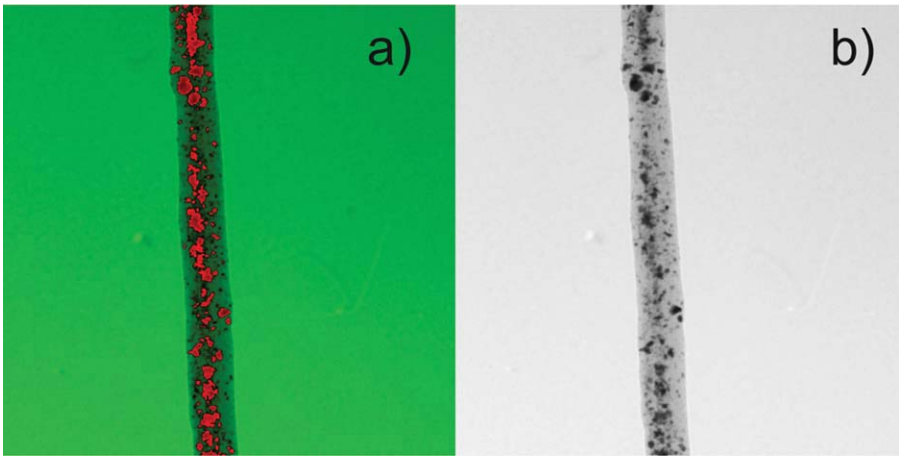

Figure 3 3D reconstructions of nanocomposite fibers obtained through Image J software: (a) Fe_3O_4 particles are evidenced through digital filtering and highlighted in red, and (b) Fe_3O_4 particles are reported in white into a gray PCL matrix. [Color figure can be viewed in the online issue, which is available at wileyonlinelibrary.com.]

observe that mechanical properties of these scaffolds (Table I) were in the range of those related to trabecular bone. Therefore, the variation in the amount of nanoparticles may be a useful tool for tailoring mechanical features.

Figure 4 shows the imaging through optical microscopy of the investigated scaffolds.

Optical imaging showed that the fibers composing the scaffold were very well aligned and regularly spaced along each layer; this suggested proper performance of the fiber-deposition process. Moreover, a 100% interconnectivity among macropores was observed. Therefore, morphologically controlled composite scaffolds based on a PCL matrix can be fabricated in similar fashion to neat PCL structures.[16,42,43]

Magnetization analysis

The magnetization curves, as shown in Figure 5, showed a superparamagnetic behavior for these PCL scaffolds containing 10 wt % magnetic Fe_3O_4 nanoparticles. The particle moment (μ_p), estimated from eq. (1), was about 10^6 μ_B. As each Fe_3O_4 molecule carried a magnetic moment of 4.7 μ_B, we estimated the particle diameter to be about 28 nm, which was equivalent to a particle mass of about 2×10^5 Fe_3O_4 molecules. This agreed well with the grain diameter provided by the producer. This further suggested a mass concentration of nanoparticles of $N = M_s/\mu_p \approx 1.5 \times 10^{15}$ particles per gram.

Even if the saturation value was low if compared to a dip-coated scaffold,[12] it was still encouraging

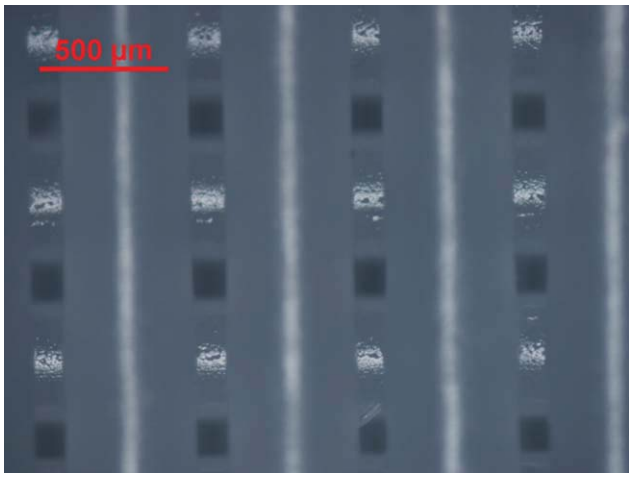

Figure 4 Optical microscopy image of a PCL/Fe_3O_4 scaffold showing that fibers composing the scaffold were very well aligned and regularly spaced along each layer and, thus, suggested proper performance of the 3D fibers deposition process. [Color figure can be viewed in the online issue, which is available at wileyonlinelibrary.com.]

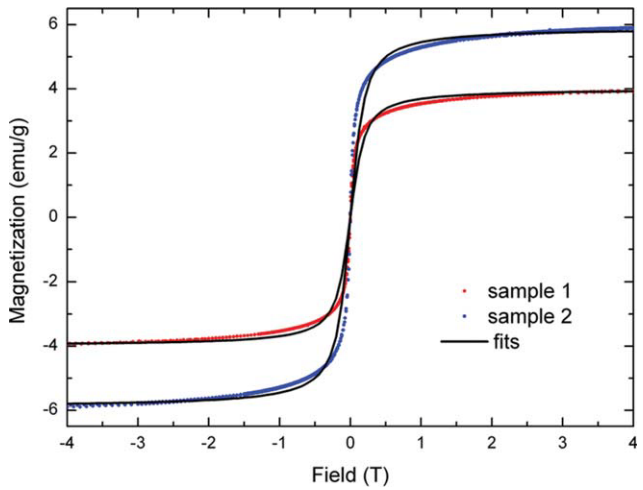

Figure 5 Magnetic moment per mass measured at 310 K for two different PCL/Fe_3O_4 samples. The black solid lines represent fits of the Langevin function to the experimental data points. [Color figure can be viewed in the online issue, which is available at wileyonlinelibrary.com.]

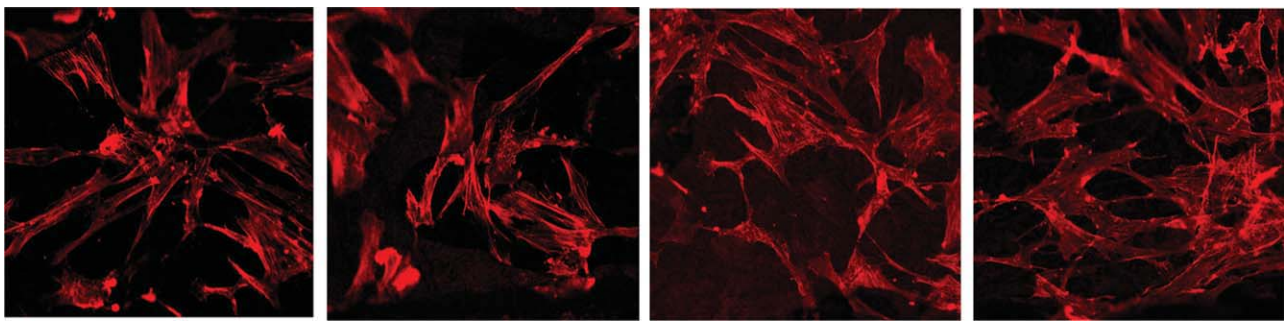

Figure 6 Images obtained from confocal analysis with several steps along the length of the nanocomposite fibers, highlighting the phalloidin-labeled actin filaments. [Color figure can be viewed in the online issue, which is available at wileyonlinelibrary.com.]

because these scaffolds could be attracted and fixed by a magnetic field [Fig. 1(b)] and they were capable of attracting the scaffold through the fully interconnected porosity (Fig. 3) obtained through rapid prototyping techniques, magnetized bioaggregates used for scaffold functionalization.

Confocal laser scanning microscopy

Confocal images showed interesting results in terms of cell adhesion and spreading (Figs. 6 and 7). Hence, preliminary studies suggest a high ability of the magnetic scaffolds to support adhesion and proliferation of human bone marrow stem cells, at least *in vitro.* Therefore, this new type of scaffold is a valuable candidate for tissue engineering applications and offers novel magnetic options.

In particular, confocal analysis highlighted an increase in the adhered number and a more evident spreading of human mesenchymal stem cells when compared to the results usually obtained from only PCL fibers.[41] This could have probably been due to the presence of Fe_3O_4 nanoparticles or to the surface topography and roughness of the nanocomposite fibers. With regard to the release of nanoparticles, several *in vitro* and *in vivo* investigations have already confirmed that magnetic nanoparticles with adequate biocompatible coatings do not have cytotoxic effects on cell development.[57] Furthermore, some magnetic nanoparticles coated with arginine-glycine-aspartic acid (RGD) peptides showed good biocompatibility in contact with osteoblasts.[58] Dobson[59] also highlighted that the change in the magnetic properties of magnetic nanoparticles in the presence of a magnetic field had no influence on cellular toxicity. However, further research is needed to asses whether this enhanced cell-material behavior is related to the presence of magnetic Fe_3O_4 powder or to changes in the topography of fibers due to the presence of nanoparticles.

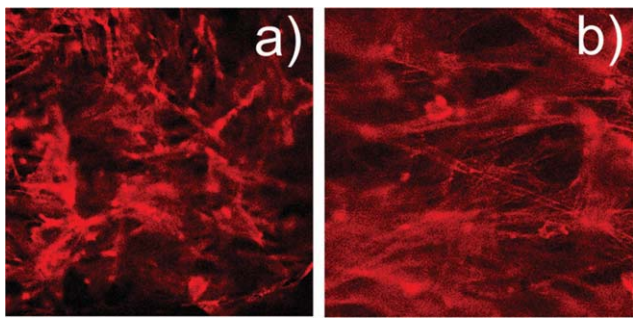

Figure 7 Image obtained from confocal analysis (a) evidencing the great number of cells adhered to the scaffold and (b) a higher magnification of the central zone reported in part a. [Color figure can be viewed in the online issue, which is available at wileyonlinelibrary.com.]

CONCLUSIONS

Completely interconnected nanocomposite magnetic scaffolds were successfully prototyped through 3D fiber deposition. An amount of 10 wt % of nanoparticles allowed for increases in the stiffness and strength of the scaffold and provided magnetic features that allowed for the design of novel fixation methods and functionalization of the scaffold, thus providing novel strategies for designing scaffolds for bone tissue engineering. Moreover, a biological *in vitro* investigation suggested an increase in the adhered number and a marked spreading of human mesenchimal stem cells.

The authors gratefully acknowledge MAGISTER Magnetic Scaffolds for *in vivo* Tissue Engineering VII PQ project NMP-2007-4.2.3.-1. The authors also thank G. Ametrano for performing the micro-CT imaging.

References

1. Langer, R.; Vacanti, J. P. Science 1993, 260, 920.
2. Raimondi, M. T.; Moretti, M.; Cioffi, M.; Giordano, C.; Laganà, F. K.; Pietrabissa, R. Biorheology 2006, 43, 215.
3. Giordano, C.; Causa, F.; Candiani, G. J Appl Biomater Biomech 2006, 4, 73.
4. Brochhausen, C.; Zehbe, R.; Gross, U.; Schubert, H.; Kirkpatrick, C. J. J Appl Biomater Biomech 2007, 5, 70.

5. Guarino, V.; Causa, F.; Ambrosio, L. J Appl Biomater Biomech 2007, 5, 149.
6. Giordano, C.; Causa, F.; Di Silvio, L.; Ambrosio, L. J Mater Sci Mater Med 2007, 18, 653.
7. Causa, F.; Netti, P. A.; Ambrosio, L. Biomaterials 2007, 28, 5093.
8. Perale, G.; Bianco, F.; Giordano, C.; Matteoli, M.; Masi, M.; Cigada, A. J Appl Biomater Biomech 2008, 6, 1.
9. Nair, K.; Yan, K. C.; Sun, W. J Appl Biomater Biomech 2008, 6, 35.
10. Haparanta, A. M.; Koivurinta, J.; Hamalainen, E. R.; Kellomaki, M. J Appl Biomater Biomech 2008, 6, 89.
11. Cigada, A. J Appl Biomater Biomech 2008, 6, 127.
12. Pertici, G.; Maccagnan, S.; Mueller, M.; Rossi, F.; Daniele, F.; Tunesi, M.; Perale, G. J Appl Biomater Biomech 2008, 6, 186.
13. Giordano, C.; Causa, F.; Bianco, F.; Perale, G.; Netti, P. A.; Ambrosio, L.; Cigada, A. Int J Artif Organs 2008, 31, 1017.
14. Perale, G.; Pertico, G.; Giordano, C.; Daniele, F.; Masi, M.; Maccagnan, S. J Appl Polym Sci 2008, 108, 1591.
15. Acetti, D.; D'Arrigo, P.; Giordano, C.; Macchi, P.; Servi, S.; Tessaro, D. Int J Artif Organs 2009, 32, 204.
16. Gloria, A.; Russo, T.; De Santis, R.; Ambrosio, L. J Appl Biomater Biomech 2009, 7, 141.
17. Hutmacher, D. W. J Biomater Sci Polym E 2001, 12, 107.
18. Hutmacher, D. W.; Schantz, T.; Zein, I.; Ng, K. W.; Teoh, S. H.; Tan, K. C. J Biomed Mater Res 2001, 55, 203.
19. Hacker, M. C.; Mikos, A. G. Tissue Eng 2006, 12, 2049.
20. Sachlos, E.; Czernuske, J. T. Eur Cell Mater 2003, 5, 29.
21. Peltola, S. M.; Melchels, F. P. W.; Grijpma, D. K.; Kellomäki, M. Ann Med 2008, 40, 268.
22. Chu, T. M. G. In Solid freeform fabrication of tissue engineering scaffoldsm, Ma, P. X., Elisseeff, J., Eds.; Taylor & Francis: Boca Raton, FL, 2006; p 139.
23. Schugens, C.; Grandfils, C.; Jerome, R.; Teyssie, P.; Delree, P.; Martin, D.; Malgrange, B.; Moonen, G. J Biomed Mater Res 1995, 29, 1349.
24. Ragaert, K.; Cardon, L.; Dekeyser, A.; Degrieck, J. Biofabrication 2010, 2, 1.
25. Fedchenko, R. P.; Jacobs, P. F. In Stereolithography and other RP&M technologies, Fedchenko, R. P., Jacobs, P. F., Eds.; Society of Manufacturing Engineers: Dearborn, MI, 1996; p 1.
26. Jacobs, P. F. In Stereolithography and other RP&M technologies, Fedchenko, R. P., Jacobs, P. F., Eds.; Society of Manufacturing Engineers: Dearborn, MI, 1996; p 317.
27. Nair, L. S.; Laurencin, C. T. Adv Biochem Eng Biotechnol 2006, 102, 47.
28. Hayashi, T. Prog Polym Sci 1994, 19, 663.
29. Griffith, L. G. Acta Mater 2000, 48, 263.
30. Burg, K. J. L.; Porter, S.; Kellam, J. F. Biomaterials 2000, 21, 2347.
31. LeGeros, R. Z. Clin Orthop Relat Res 2002, 395, 81.
32. Mikos, A. G.; Sarakinos, G.; Leite, S. M.; Vacanti, J. P.; Langer, R. Biomaterials 1993, 14, 323.
33. Freed, L. E.; Vunjak-Novakovic, G.; Biron, R. J.; Eagles, D. B.; Lesnoy, D. C.; Barlow, S. K.; Langer, R. Biotechnology (NY) 1994, 12, 689.
34. Chang, B. S.; Lee, C. K.; Hong, K. S.; Youn, H. J.; Ryu, H. S.; Chung, S. S.; Park, K. W. Biomaterials 2000, 21, 1291.
35. Jin, Q. M.; Takita, H.; Kohgo, T.; Atsumi, K.; Itoh, H.; Kuboki, Y. J Biomed Mater Res 2000, 51, 491.
36. Shalak, R.; Fox, C. F. In Tissue engineering, Shalak, R., Fox, C. F., Eds.; Liss: New York, 1988; p 26.
37. Zhong, Z. K.; Sun, X. Z. S. Polymer 2001, 42, 6961.
38. Allen, C.; Han, J.; Yu, Y.; Maysinger, D.; Eisenberg, A. J Controlled Release 2000, 63, 275.
39. Ng, K. W.; Hutmacher, D. W.; Schantz, J. T.; Ng, C. S.; Too, H. P.; Lim, T. C.; Phan, T. T.; Teoh, S. H. Tissue Eng 2001, 7, 441.
40. Hutmacher, D. W.; Schantz, T.; Zein, I.; Ng, K. W.; Teoh, S. H.; Tan, K. C. J Biomed Mater Res 2001, 55, 203.
41. Causa, F.; Battista, E.; Della Moglie, R.; Guarnieri, D.; Iannone, M.; Netti, P. A. Langmuir 2010, 26, 9875.
42. Kyriakidou, K.; Lucarini, G.; Zizzi, A.; Salvolini, E.; Mattioli Belmonte, M.; Mollica, F.; Gloria, A.; Ambrosio, L. J Bioact Compat Polym 2008, 23, 227.
43. Gloria, A.; De Santis, R.; Ambrosio, L. J Appl Biomater Biomech 2010, 8, 57.
44. Tran, N.; Webster, T. J. WIREs Nanomed Nanobiotechnol 2009, 1, 336.
45. Webster, T. J.; Siegel, R. W.; Bizios, R. Biomaterials 1999, 20, 1221.
46. Webster, T. J.; Siegel, R. W.; Bizios, R. Biomaterials 2000, 21, 1803.
47. Liu, H.; Slamovich, E. B.; Webster, T. J. Nanotechnology 2005, 16, 601.
48. Rogel, M. R.; Qiu, H.; Ameer, G. A. J Mater Chem 2008, 18, 4233.
49. Du, C.; Cui, F. Z.; Zhu, X. D.; de Groot, K. J Biomed Mater Res 1999, 44, 407.
50. Du, C.; Cui, F. Z.; Feng, Q. L.; Zhu, X. D.; de Groot, K. J Biomed Mater Res 1998, 42, 540.
51. Boccaccini, A. R.; Roether, J. A.; Hench, L. L.; Maquet, V.; Jerome, R. Ceram Eng Sci Proc 2002, 23, 805.
52. Marra, K. G.; Szem, J. W.; Kumta, P. N.; Di Milla, P. A.; Weiss, L. E. J Biomed Mater Res 1999, 47, 324.
53. Kalita, S.; Finley, J.; Bose, S.; Hosick, H.; Bandyopadhyay, A. Mater Res Soc Symp Proc 2002, 726, 91.
54. Blaker, J. J.; Gough, J. E.; Maquet, V.; Notingher, I.; Boccaccini, A. R. J Biomed Mater Res A 2003, 67, 1401.
55. Bock, N.; Riminucci, A.; Dionigi, C.; Russo, A.; Tampieri, A.; Landi, E.; Goranov, V. A.; Marcacci, M.; Dediu, V. Acta Biomater 2010, 6, 786.
56. De Santis, R.; Ambrosio, L.; Mollica, F.; Netti, P.; Nicolais, L. In Modeling of Biological Materials; Mollica, F., Preziosi, L., Rajagopal, K. R., Eds.; Birkhauser: Boston, 2007.
57. Butoescu, N.; Seemayer, C. A.; Foti, M.; Jordan, O.; Doelker, E. Biomaterials 2009, 30, 1772.
58. Hughes, S.; Dobson, J.; El Haj, A. J. J Biomech 2007, 40, S96.
59. Dobson, J. Nat Nanotechnol 2008, 3, 139.